J. Plasma Physics (2009), *vol.* 75, *part* 6, *pp.* 799–815. © Cambridge University Press 2009
doi:10.1017/S0022377809007934

Ultra-cold plasmas: a paradigm for strongly coupled and classical electron fluids

CLAUDE DEUTSCH[1], GUENTER ZWICKNAGEL[2] and ANTOINE BRET[3]

[1]LPGP (UMR-CNRS 8578), Bât. 210, UPS, 91405 Orsay, France

[2]Institut fuer Theoretische Physik II, Staudtstr. 7, 91058 Erlangen, Germany

[3]ETSI Industriales, Universidad de Castilla, La Mancha, 13071 Ciudad Real, Spain

(Received 7 January 2009, revised 22 February 2009 and accepted 23 February 2009, first published online 15 April 2009)

Abstract. Ultra-cold plasmas obtained by ionization of atomic Rydberg states are qualified as classical and strongly coupled electron fluids. They are shown to share several common trends with ultra-cold electron flows used for ion-beam cooling. They exhibit specific stopping behaviour to charged particle beams, which may be used for diagnostic purposes. Ultra-cold plasmas are easily strongly magnetized. Then, one expects a strongly anisotropic behaviour of low ion velocity slowing down when the target electron cyclotron radius becomes smaller than the corresponding Debye length.

1. Introduction

We intend to review some conspicuous features of the ultra-cold plasma (UCP) observed in the quasi-reversible transformation of cold atomic Rydberg states into an expanding fluid of free electrons neutralized by much slower residual ions. Such a process is routinely observed since the first unambiguous identification due to Vitrant et al. [1] as early as 1982. In the meantime, many accurate experiments [2–6], performed on both sides of the Atlantic, have definitively settled an unexpected territory in the temperature–density plane of current use by plasma physicists. However, it seems to us that the potentialities of cross fertilization afforded by a very unusual interplay of atomic physics with plasma collective phenomena have been largely under appreciated, up to now.

Such a view explains the organization of the present work. In Sec. 2, we recall in a non-technical presentation the physics of atomic cooling. This section is meant essentially for a plasma physicists readership.

In Sec. 3, we show how the inclusion of binary particle correlation leads to specific modellings of the expanding UCP. Sections 4 and 5 advocate charged particle stopping and energy loss in the UCP as a possible diagnostic method.

A first approach when no applied magnetic field is present ($B = 0$) is presented in Sec. 4, while the strongly magnetized case ($B \neq 0$ and $\omega_c \geqslant \omega_p$) is detailed in Sec. 5. Then, specific attention is given to low ion velocity slowing down (LIVSD) in terms of the target plasma hydromodes. Conclusion and outlook are offered in Sec. 6.

https://doi.org/10.1017/S0022377809007934 Published online by Cambridge University Press

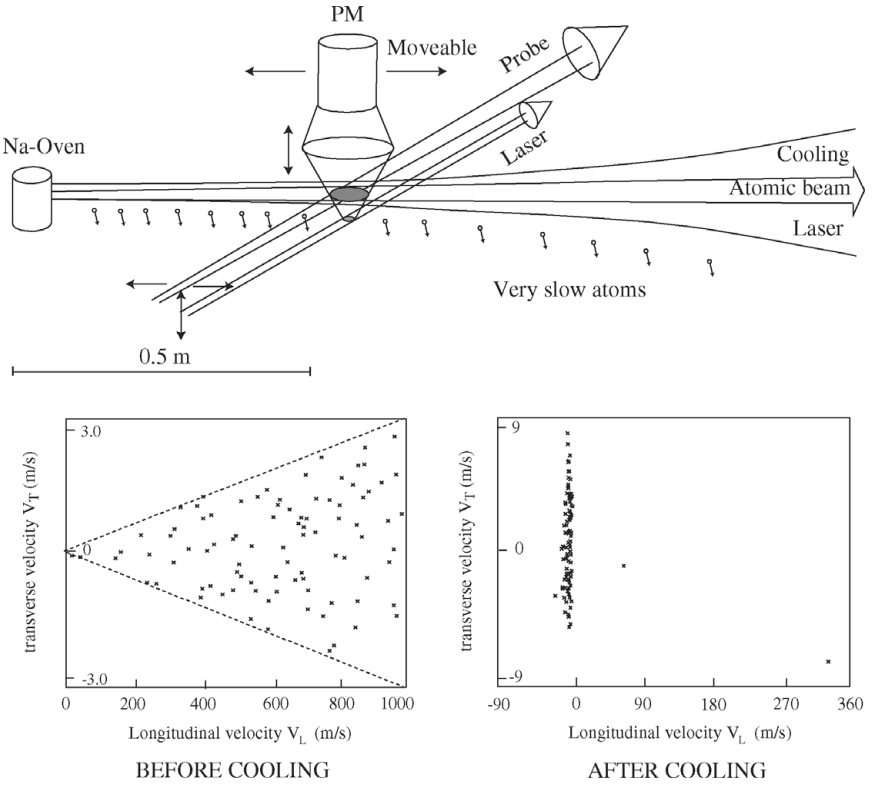

Figure 1. Particle slowing down using chirped laser frequency.

2. Atomic cooling and ultra-cold plasma formation

We sketch here briefly for non-specialists the basic concepts underlining the production of UCP through laser cooling of atomic species. We do so in a non-technical way through a few selected pictures.

In Fig. 1, we picture a typical laser cooling process of Na atoms.

Toward this goal one uses a tunable laser and triggers the laser frequency well below the natural frequency. Photons of this low frequency will interact with the high-speed particles in the beam, slowing them down. The frequency of the laser is then increased so that the slowed atoms and those atoms with a lower initial velocity are both slowed. As the laser continues to 'chirp' upward in frequency, it sweeps the velocity of all the particles downward. Then, all the particles in the beam are slowed down to the same velocity. In Fig. 1, Na atoms come from an oven with a wide spread in initial longitudinal and transverse velocities. As depicted in 'before cooling' and 'after cooling' scatter diagrams, the chirped laser sweeps all the atoms but two to zero longitudinal frequency. The chirped laser light brings the sodium beam to a stop and converts it into a slowly expanding cloud of Na atoms with a density $\sim 10^6$ atoms/cc with an expanding velocity ~ 6 m/s equivalent to a 50 mK kinetic temperature.

Neutral particles are likely to remain in their ground state. They can be excited to a higher state by a laser tuned to the resonance frequency corresponding to the

https://doi.org/10.1017/S0022377809007934 Published online by Cambridge University Press

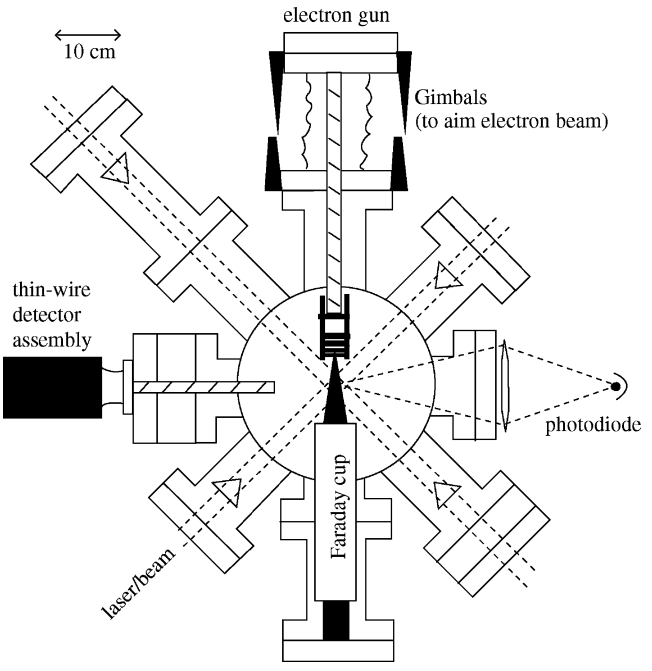

Figure 2. Magneto-optical traps. A standard display including an electron beam for atomic excitation [7].

transition to that state. The laser photons needed to excite the first excited states for atomic and molecular hydrogen are in the vacuum ultraviolet (VUV) region.

Actually, the production of UCP [2–6] is obtained by combining three pairs of laser beams acting in conjunction with an inhomogeneous magnetic field on alkali (Rb for instance) atoms.

A standard setup is pictured in Fig. 2. It also includes an electron beam for excitation of atomic levels [7].

In Fig. 2, the six laser beams (one pair is out of the screen) combined with an inhomogeneous magnetic field trap 10^6 atoms, in a ball about 1/2 mm in diameter. The relative number of atoms trapped is measured by the Rb (5p to 5s) fluorescence using the photodiode. The trapping lasers are turned off, and the electron beam is pulsed on. After a short delay, the trapping lasers are turned on. The decrease in Rb fluorescence is proportional to the number of atoms lost from the trap due to being hit by an electron. By knowing the electron current density at the trap and the fraction of atoms lost from the trap various cross sections can be determined.

Some experimental specifications for this case run as follows:

Atoms in trap	10^6 atoms at 100 μK
Electron energy range	0 to 500 eV
Electron beam current	150 μA at 100 eV

In experiments performed very recently by Li et al. [8], one starts with ^{85}Rb atoms in a vapour-loaded magneto-optical trap (MOT), in which the atoms are at 300 μK and at $5p_{3/2}$ density of 5×10^{10} cm^{-3}. The atoms are excited from the $5p_{3/2}$ state to ns or nd Rydberg states at a 20 Hz repetition rate using a pulse-amplified, frequency-doubled 960 nm continuous-wave Ti:sapphire laser. The laser

https://doi.org/10.1017/S0022377809007934 Published online by Cambridge University Press

pulses have a 10 ns duration, a 20 μJ energy, and a 200 MHz bandwidth, and the beam is focused to a 0.2 mm diameter waist in the trap volume. About 10% of the cold atoms are excited to Rydberg states, leading to a maximum density of Rydberg atoms of 5×10^9 cm^{-3}.

The plasma formation is observed and also population transfer to higher dipole coupled states starting from initially excited Rb ns and nd states as a function of Rydberg atom density and time delay after laser excitation. One analyses the final states of the atoms by applying a field ramp with a rise time of 2 μs. The ions or electrons in an UCP are detected at the beginning of the field ramp, and the atoms in a Rydberg state are detected after the ramped field reaches its ionization threshold. In the time-resolved signals, it is straightforward to observe ionization and state changing using electron detection.

Li et al. [8] interpreted their observations as follows.

In cold dense Rydberg atom samples, the dipole–dipole interaction strength appears resonant at the typical interatomic spacing in the sample, and the interaction has a $1/R^3$ dependence on the interatomic spacing R. The dipole–dipole attraction leads to ionizing collisions of initially stationary atoms, which produces hot atoms and ions and initiates the evolution of initially cold samples of neutral Rydberg atoms into plasmas. More generally, the strong dipole–dipole forces lead to motion.

3. Dense and strongly coupled electron fluid

3.1. A bit of numerology

A priori, the very low particle densities observed in the expanding UCP could lead to a neglect of particle–particle correlations.

Such a view has been very recently stressed by Comparat et al. [9] through an intriguing analogy between expanding UCP and gravitational equilibrium of globular star clusters. These authors also advocated a time evolution monitored by a Fokker–Planck kinetic equation putting in parallel binary star formation and three-body recombination into Rydberg atoms. Such an approach might be well suited for the description of these atomic and local processes, where correlations are not fundamentally involved. However, to investigate genuine plasma physics implying collective effects, one needs to include particle correlations.

Here, we proceed to a standard analysis for qualifying the UCP phases in a density–temperature framework. In view of the Coulomb and long-range interactions, it is recommended to evaluate carefully binary correlations between particles within the UCP electron fluid. Such correlations are qualified for particles obeying classical Boltzmann statistics by the dimensionless parameter

$$\Gamma = \frac{(Ze)^2}{aT} = 2.69 \times 10^{-5} Z^2 \left(\frac{n_e}{10^{12}\ \text{cm}^{-3}} \right)^{1/3} \left(\frac{T_e}{10^6\ \text{K}} \right)^{-1}, \tag{1}$$

with $a = (4/3\pi n_e)^{-1/3}$ meaning interelectron distances and Z denoting the ion charge neutralizing the UCP.

UCP maintains such a low T_e as soon as $n_e \geqslant 10^6$ cm^{-3}, $\Gamma \geqslant 0.2$, a fiducial figure for most expanding UCP encountered in the literature. Therefore, it is appropriate to include correlation effects in any quantitative estimate of equilibrium or transport UCP properties.

https://doi.org/10.1017/S0022377809007934 Published online by Cambridge University Press

Simultaneously, at the n_e values considered, the Wigner parameter

$$r_s = \frac{a}{r_B} \approx \left[\frac{n_e}{1.6 \times 10^{24}\ \mathrm{cm}^{-3}}\right]^{1/3} \tag{2}$$

measuring a in numbers of the Bohr radius r_B remains always much larger than one, which pertains to a classical UCP, fulfilling Boltzmann statistics. This feature is at variance with usual partially degenerate electron fluid [10] neutralizing and polarizing as well as classical and strongly coupled ions with much larger n_e values.

This a priori paradoxical situation is also highlighted by the degeneracy parameter

$$\Theta = \frac{k_B T_e}{E_F} = \frac{2 m_e k_B T_e}{\hbar^2 (3\pi^2 n_e)^{2/3}}$$

$$= 2\left(\frac{4}{9\pi}\right)^{2/3} \frac{r_s}{\Gamma} \tag{3}$$

also being much larger than one.

3.2. Time evolution

Most of the significant physics encountered in the Rydberg–UCP transition has to do with the expansion of the initial ultra-cold atoms and their subsequent ionization. So, comprehending intricacies of the plasma phase time development appears as a basic challenge involving dynamical correlations between charged particles. Hopefully, the given UCP expansion may be rather convincingly modelled through adequate molecular dynamics (MD) numerical simulations [11], provided that the ultraviolet divergence associated with the short-range electron–ion interaction is carefully taken care of. An accurate albeit simple expression validated by many applications reads [12]

$$V_{\alpha\beta}(r) = \frac{Z_\alpha Z_\beta e^2}{4\pi e_0} \frac{1 - \exp(-\kappa_{\alpha\beta} r)}{r}, \quad V_{\alpha\beta}(0) = \frac{Z_\alpha Z_\beta e^2}{4\pi e_0} \kappa_{\alpha\beta}, \tag{4}$$

with $\kappa_{\alpha\beta} = 2\pi/\lambda_{th}(\mu_{\alpha\beta})$ for a hydrogenic pair with charges Z_α and Z_β and thermal de Broglie wavelength $\lambda_{th}(\mu_{\alpha\beta}) = \hbar/\sqrt{2m\mu_{\alpha\beta} k_B T}$, where $\mu_{\alpha\beta} = m_\alpha m_\beta/(m_\alpha + m_\beta)$. Interaction (4) is plotted in Fig. 3 as

$$\frac{\bar{V}(r)}{\bar{V}(0)} = \frac{1 - \exp(-\kappa r)}{\kappa r}, \tag{5}$$

contrasted to the approximation

$$\frac{\bar{V}(\mathrm{r})}{\bar{V}(0)} = \begin{cases} \dfrac{(\kappa r)^2}{27} - \dfrac{\kappa r}{3} + 1, & \kappa r < 3, \\ \dfrac{1}{\kappa r}, & \kappa r \geqslant 3. \end{cases} \tag{6}$$

Time evolution per se is displayed in Fig. 4 for potential energy U_{pot} and temperatures renormalized by the thermal temperature T ($= T_e = T_i$) at two distinct Γ values. Running time t is given in numbers of $\tau_p = \omega_p^{-1}$ with $\omega_p^2 = 4\pi Z_\alpha^2 n_e e^2/m_e$. The weak-coupling case (Fig. 4a) advocates steady temperatures $T_e \# T_i$ and $U_{pot} \geqslant 0$. The correlated situation (Fig. 4b) looks very different. The ion temperature remains constant as previously. However, the electron temperature T_e steadily

https://doi.org/10.1017/S0022377809007934 Published online by Cambridge University Press

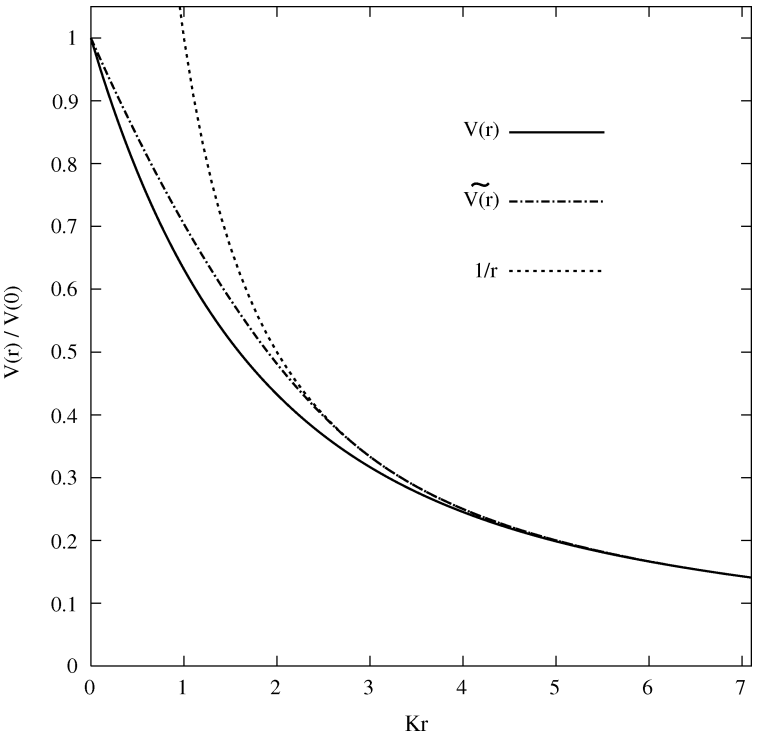

Figure 3. Effective electron–ion interaction (4).

increases as a result of partial three-body recombination into Rydberg atoms, while $U_{\rm pot}$ becomes more and more negative.

At large t, one can expect that colder ions mimic the homogeneous and rigid neutralizing background in the one-component plasma (OCP) models [13].

3.3. Rydberg matter

Another aspect of a two-component plasma (TCP) electron–ion system featuring extensively the impact of Coulomb correlation on the plasma structure is the building up of the elusive phase of Rydberg matter. Again, we shall rely on numerical simulations conducted very recently by Bonitz et al. [14] in the framework of the path-integral Monte Carlo (PIMC) scheme [15] for investigating internal energy pressure and pair correlation functions in the temperature range $T = 0.1$–10 K with $n_{\rm e} = 10^9$–10^{15} cm^{-3}, spanning densities somewhat larger than those currently accessible to present laboratory UCPs. At small Γ (Fig. 5), the considered TCP remains clustered into quasi-molecules [14] featuring a few point-like charges of either sign (see part (c) of Fig. 5).

Such a configuration retains only short-range ordering. On the other hand, at high Γ ($\gg 1$), a reticulated organization takes place with either electrons or ions (part (a) of Fig. 5) on the same quasi-lattice sites, or on distinct quasi-lattice sites (part (b) of Fig. 5). These conspicuous numerical expectations are still awaiting a decisive confrontation with bona fide experimental results. It should be finally appreciated that the reticulated systems (a) and (b) in Fig. 5 are not genuine crystalline structures with infinite propagation of the long range positional order.

https://doi.org/10.1017/S0022377809007934 Published online by Cambridge University Press

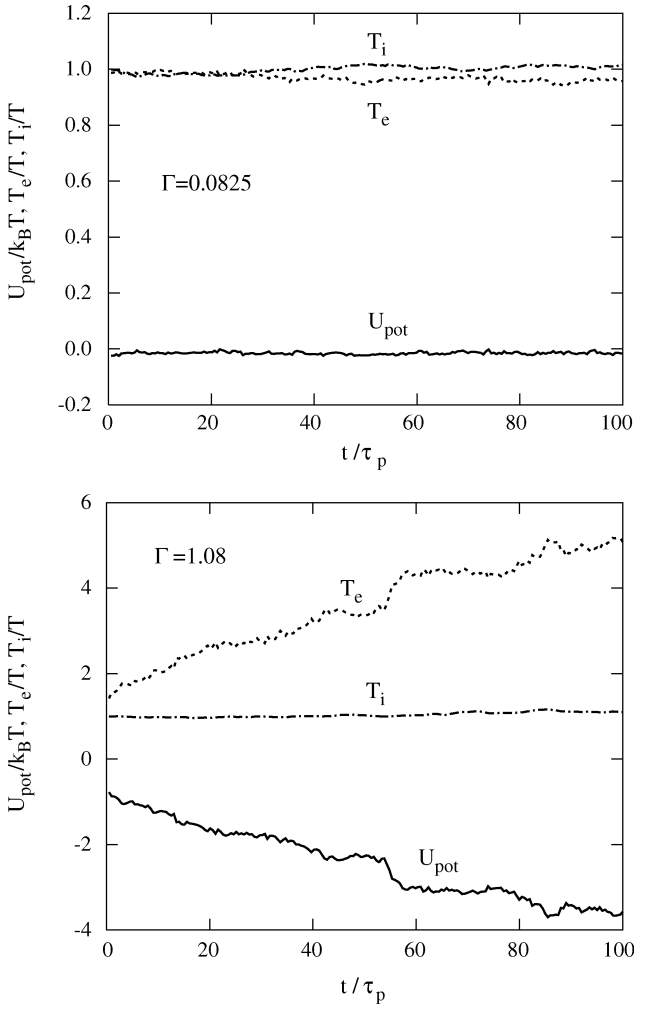

Figure 4. Temporal evolution of particle temperatures and potential energies in weakly [(a) $\Gamma = 0.0825$] and coupled [(b) $\Gamma = 1.08$] plasmas under three-body recombination.

Also, the given electronic component significantly departs from the conduction band of alkali metals, the closest realization of the OCP model in the laboratory. The alluded to difference arises from the strong density inhomogeneity of the electron fluid made of particles spending a lot of time very far from their parent nuclei (Rydberg atom structure).

4. Ion stopping in ultra-cold plasmas ($B = 0$)

Up to now, only a few classical electron fluids have been identified experimentally. One of them which seems to share a lot of common features with the UCP of the present interest is the electron flow used for cooling of energetic ion beams (Fig. 6). Very cold electrons stream parallel (or sometimes antiparallel) to the ion beam in a

https://doi.org/10.1017/S0022377809007934 Published online by Cambridge University Press

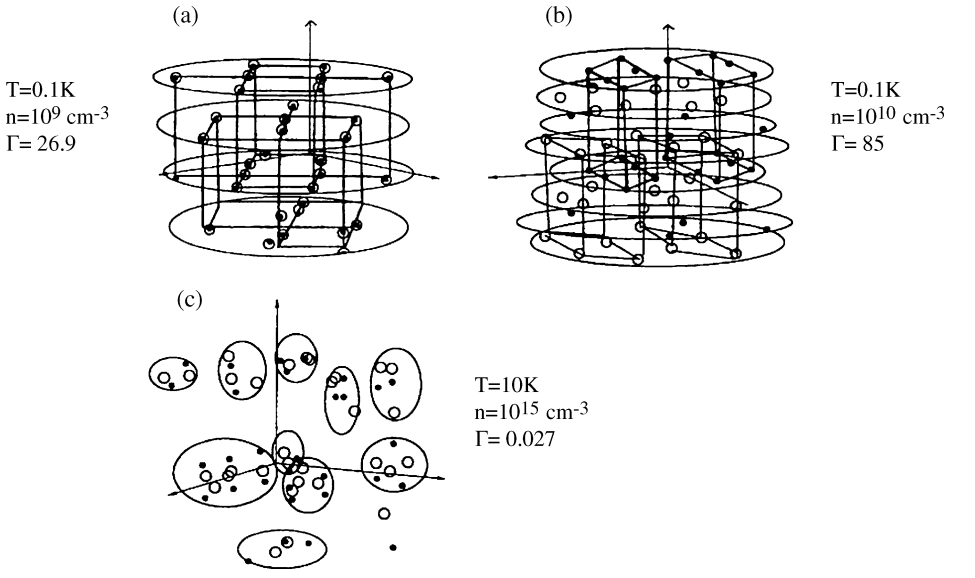

Figure 5. Rydberg matter particle coordinates pertaining to pair correlation functions $g_{ee}(r)$, $g_{ii}(r)$, and $g_{ei}(r)$. Open and filled circles represent ions and electrons, respectively: (a) $T = 0.1$ K, $r = 10^9$ cm^{-3}, ions and electrons sit on the same lattice sites, (b) $T = 0.1$ K, $n = 10^{10}$ cm^{-3}, ions and electrons sit on distinct lattice sites, (c) $T = 0.1$ K, $n = 10^{15}$ cm^{-3}, ions and electrons cluster into droplets [14].

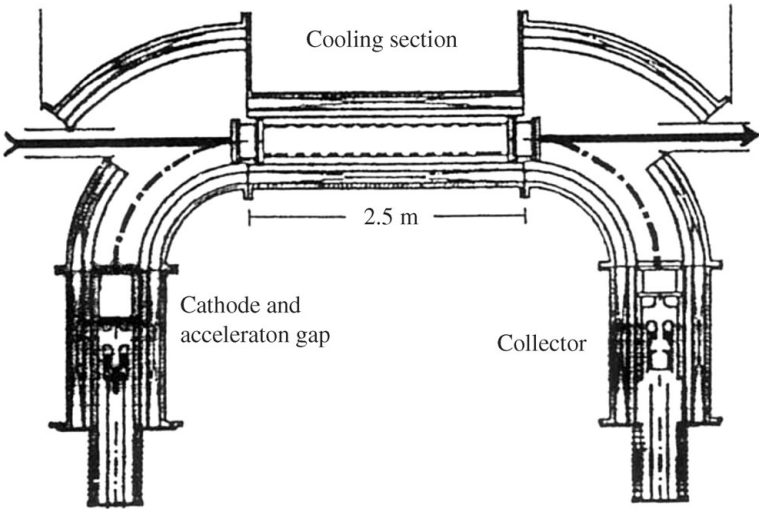

Figure 6. Heidelberg Test Storage Ring (TSR). Electron cooling device. Electron energies can be varied between 2 and 320 keV with a maximum design current of 10 A. The e-beam diameter is 5 cm and the length of the electron–ion interaction region 250 cm.

given accelerating structure, to reduce the ion beam emittance (transverse entropy), while raising it in the electron beam.

The quantitative understanding of the cooling process is well documented by now. It essentially relies on a careful understanding of ion beam stopping and energy loss into the parallel electron fluid.

https://doi.org/10.1017/S0022377809007934 Published online by Cambridge University Press

There are two conventional approaches to the stopping power, the dielectric linear response (DLR) formalism and the binary collision treatment. In the dielectric description the stopping power dE/ds is calculated as the force between the ion and the polarization cloud created by the ion and can be expressed in terms of the dielectric function $\varepsilon(\kappa,\omega)$:

$$-\frac{dE}{ds}\frac{\lambda_{\rm D}}{\kappa_{\rm B}T} = Z_{\rm p}^2\sqrt{3}\Gamma^{3/2}\frac{\lambda_{\rm D}^2}{2\pi^2}\times\int_{\kappa<\kappa_{\rm m}} d^3\kappa\frac{\kappa\cdot\hat{v}}{\kappa^2}Im\left[\frac{1}{\varepsilon(\kappa,\kappa\cdot v)}\right], \tag{7}$$

where v = projectile velocity.

For classical systems the dielectric function ε can be written in terms of the Fried–Conte plasma dispersion function and represents the limit $\hbar\to 0$ of the classical random phase approximation (RPA) dielectric function for any degeneracy of the electron target. The classical linear response description, however, cannot treat close ion–electron collisions. To correct for this, a cut-off $k_{\rm m}$ is introduced to incorporate a Bloch correction for the stopping power which accounts for the contribution of close collisions in an approximate manner for $|Z_{\rm p}|\Gamma^{3/2}/(1+(v/v_{\rm th})^3)\ll 1$. For classical ion–electron collisions with $n>1$ this cut-off is given by $\kappa_{\rm m}\approx 1/\langle b_0\rangle = 4\pi\varepsilon_0 m\langle v_{\rm r}\rangle^2/|Z_{\rm p}|e^2 = (1+v^2/v_{\rm th}^2)/\sqrt{3}|Z_{\rm p}|\Gamma^{3/2}\lambda_{\rm D}$.

$\lambda_{\rm D}$ is the usual target electron Debye length $\lambda_{\rm D}=(k_{\rm B}T/4\pi n_{\rm e}e^2)^{1/2}$.

In the binary collision approach (BCA) the stopping power is obtained as the average over the momentum transfer in isolated collisions between the ion and target electrons. In terms of the transport cross section $\sigma_{\rm tr}$ for the ion–electron collisions, the stopping power dE/ds (in KbT/Debye length) on heavy ions (i.e. in the limit of an infinite projectile mass) reads

$$-\frac{dE}{ds}\frac{\lambda_{\rm D}}{\kappa_{\rm B}T} = \frac{Z_{\rm p}^2}{4\pi(\sqrt{3})^3}\left\{\int\frac{d^3v_{\rm r}}{2\pi^{3/2}v_{\rm th}^3}\exp\left(-\frac{(v_{\rm r}+v)^2}{2v_{\rm th}^2}\right)\frac{v_{\rm r}}{v_{\rm th}}\frac{\hat{v}\cdot v_{\rm r}}{v_{\rm th}}\frac{\sigma_{\rm tr}(v_{\rm r})}{\lambda_{\rm D}^2}\right\} \tag{8}$$

for an electron target with a Maxwell velocity distribution. $v_{\rm r}$ denotes the relative velocity between projectile and target electron.

Figure 7 exhibits stopping profiles according to (7)–(8) contrasted to molecular dynamics (MD) and Vlasov simulations, in terms of projectile velocity divided by target electron thermal velocity. The agreement between the four considered approaches deteriorates somewhat with increasing Γ value, especially for moderate or small projectile velocity. Clearly, the linear response (7) exhibits a marked correlation hole, not confirmed by other estimates [16, 17].

On the other hand, the Bethe-like high-v behaviour remains correct at any Γ. An encouraging feature of these calculations is the good agreement for all Γ and v values of simulation results obtained either through MD or particle-in-cell (PIC) simulations. This allows us to benchmark quantitatively their given stopping profiles before confrontation with experimental measurements.

In the limit of low velocities ($v\ll 1$), the stopping power behaves as

$$-\frac{dE}{ds} = R_1 v + R_3 v^3 + O(v^5),$$

where the friction coefficient R_1 in the binary collision approximation is given by

$$R_1 = Z_{\rm p}^2\Gamma^3\frac{1}{6}\frac{2}{\pi}\int_0^\infty dx\, e^{-x}\ln\left(1+\frac{4x^2}{3Z_{\rm p}^2\Gamma^3}\right). \tag{9}$$

https://doi.org/10.1017/S0022377809007934 Published online by Cambridge University Press

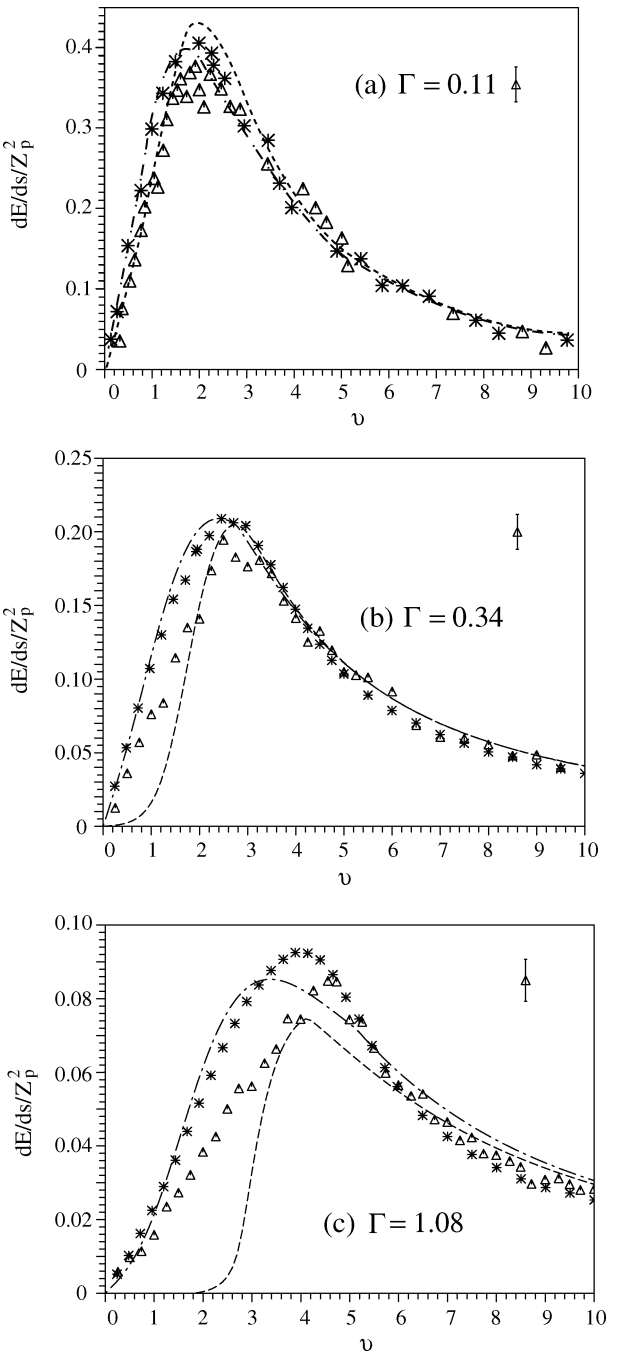

Figure 7. Normalized stopping power $dE/ds/Z_{\rm p}^2$ in units of $3^{1/2}\Gamma^{3/2}k_{\rm B}T/\lambda_{\rm D}$ as a function of the ion velocity v in $v_{\rm th} = (k_{\rm B}T/m)^{1/2}$ for an ion of charge $Z_{\rm D} = 10$ in electron plasmas with $\Gamma = 0.11$ (top), 0.34 (centre), and 1.08 (bottom): MD simulations (Δ), with typical size of error bars as indicated top right in each case, Vlasov simulations in the linear response description (7) (dashed curve), and the binary collision treatment (8) (dash–dotted).

https://doi.org/10.1017/S0022377809007934 Published online by Cambridge University Press

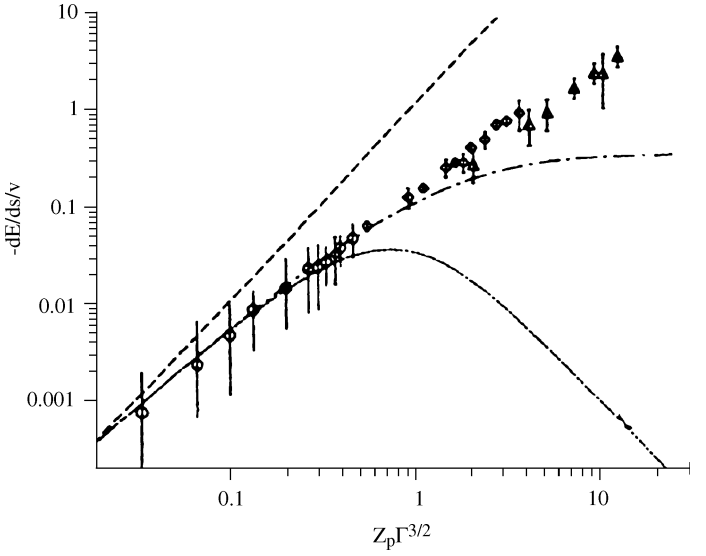

Figure 8. Friction coefficients $-dE/ds/v$ as a function of the coupling parameter $Z\Gamma^{3/2}$. Energies E and velocities v are in thermal units and distances are in Landau lengths e^2/k_bT_e. MD simulation results for $\Gamma = 0.08$ (Δ), $\Gamma = 0.34$ ($\Box$), and $\Gamma = 0.11$ ($\circ$), with error bars compared with the binary collision approximation (dash–dotted curve (9)) and the linear dielectric response treatment (dotted curve (10)). The dashed line is a pure Z_p^2 law curve.

In the dielectric linear response formalism, it is given by

$$\begin{aligned} R_1 &= -\frac{Z_p^2\Gamma^3}{3(2\pi)^{1/2}}\left[\ln(\kappa_m^2+1) - \frac{\kappa_m^2}{\kappa_m^2+1}\right], \\ \kappa_m &= \frac{2}{3^{1/2}|Z_p|\Gamma^{3/2}}. \end{aligned} \tag{10}$$

Corresponding friction coefficients $-dE/ds/v$ are graphed in terms of the coupling parameter $Z_p\Gamma^{3/2}$ in Fig. 8, together with MD simulation results and a pure Z_p^2 law curve (straight dotted line).

Again, the BCA profile fits more closely the trustable simulation results than dielectric DLR ones.

As a straightforward application of the present reasoning, let us consider the simultaneous expansion of an ion cloud surrounded by free electrons [18], with

$$\frac{V \text{ expanding heavy ion}}{V \text{ thermalized free electron}} \approx 1.2 \times 10^{-4}.$$

So, practically, we can safely state that no friction is expected between expanding ions and the expanding free electron fluid, which seems to confirm simulation results [18] for the expansion process.

For diagnostic purposes, it might be useful to consider ion projectiles with an impinging velocity v far above that of the expanding and thermalized electrons v_{th}.

https://doi.org/10.1017/S0022377809007934 Published online by Cambridge University Press

So, restricting first to a three-dimensional expansion, the above expressions (7) and (8) simplify to

$$\left(-\frac{dE}{dx}\right)_{3D} = 4\pi\frac{Z_p^2 e^4 n_e}{m_e v^2}\left(\frac{2m_e v^2}{\hbar\omega_p}\right) + O(1/v^4). \tag{11}$$

On the other hand, paying attention to a mostly planar expansion, one then has to switch to a novel situation featuring a classical 2D electron fluid.

In this case [19], the RPA has to be reworked. So, the Bethe-like expression (11) now becomes intrinsically quantum mechanical, under the form

$$-\frac{dE}{dx} = 2\pi^2\frac{Z_p^2 e^4 n_e}{\hbar V} + O(1/V^2), \tag{12}$$

with corresponding linear range for complete stopping

$$D(\mathrm{cm}) = 1.88\times 10^{-9}\frac{E_i^{3/2}}{Z^2 n_e M_e^{1/2}}, \tag{13}$$

with E_i (eV) the ion projectile energy, ion mass M in g, and target electron density n_e in cm^{-2}. For instance, 10 keV protons in a plane and a classical electron fluid with $n_e = 10^8$ cm^{-2} will experience $dE/dx \sim 0.32$ keV/cm and $D \sim 15$ cm.

The MOT pictured in Fig. 2 illustrates the interaction geometry allowing energy loss measurements for a slow electron beam stopped in a ball of UCP.

5. Low ion velocity slowing in a strongly magnetized ultra-cold plasma

It is straightforwardly observed that it is rather easy to magnetize, even strongly, an expanding UCP. This is achieved as soon as the electron cyclotron frequency fulfils $\omega_b \gg \omega_p$ with

$$B(\mathrm{G}) \gg 3.203\times 10^{-3}(n_e(\mathrm{cm}^{-3}))^{1/2}, \tag{14}$$

while the corresponding heavy-ion (Rb for instance) gyroradius $\omega_{b,i}$ is obviously fulfilling

$$\begin{aligned} r_{ci} &= v_{T_i}/\omega_{b,i} \\ &= 1.02\times 10^2 \mu^{1/2} Z^{-1} T_i^{1/2} B^{-1}\ \mathrm{cm} \gg r_L \end{aligned} \tag{15}$$

with $\mu = m_i/m_{\mathrm{proton}}$, T_i in eV, and B in gauss. r_L denotes the electron Larmor radius.

The combination of (14) and (15) highlights a strongly magnetized electron UCP neutralized by an ion fluid hardly affected by the magnetic field B.

Ion-beam stopping in a dense plasma submitted to an arbitrary large and steady magnetic field **B** is a recurrent topic encompassing a huge range of practical situations of very high interest. Here we focus attention on ultra-cold plasmas (UCPs) and cold electron setups used for ion-beam cooling.

These interaction geometries also highlight low ion velocity slowing down (LIVSD) as playing a fundamental role in asserting the confining capabilities and thermonuclear burning efficiency in dense and strongly magnetized media.

Our present goal is to demonstrate that LIVSD transverse and parallel to **B** may be given analytic expressions through a derivation free from ambiguities usually

https://doi.org/10.1017/S0022377809007934 Published online by Cambridge University Press

plaguing the most sophisticated combination of binary collision approximation and dielectric response [20]. We thus implement a radically novel approach [21] to LIVSD when the projectile velocity V remains smaller than the target electron thermal velocity $V_{\rm the}$. We thus consider ion stopping

$$S(V) \equiv \frac{dE_{\rm b}}{dx}(V) \tag{16}$$

near $V = 0$. The ratio $S(V)/V$ usually monitors a linear stopping profile, up to 100 keV/a.m.u. in cold matter. Similar trends were also reported in highly ionized plasma with $B = 0$ or $B \neq 0$ [20].

From now on, we intend to make use of a very powerful connection between very low velocity ion stopping and particle diffusion through Einstein characterization of ion mobility associated with thermal electron fluctuations in the target, around the slow ion projectile visualized as an impurity immersed in a dense and homogeneous electron fluid.

Technically, we are then led to use the recently proposed and exact Dufty–Berkovsky relationship [21, 22]

$$\lim_{V \to 0} \frac{S(V)}{V} = k_{\rm B} T_{\rm e} D^{-1} \tag{17}$$

connecting the ratio of stopping to V in the zero-velocity limit with the ion-diffusion coefficient in the target.

In a magnetized plasma D can be readily expressed in terms of Green–Kubo integrands (GKIs) involving field fluctuations in the target electron fluid, under the form

$$D = \frac{c^2}{B^2} \int_0^\infty d\tau \langle \vec{E}(\tau) \cdot \vec{E}(0) \rangle \tag{18}$$

in terms of an equilibrium canonical average of the two-point autocorrelation function for fluctuating electric fields [23, 24].

At this juncture we need to frame the GKI in suitable magnetized one component plasma (OCP) models [23, 24] for the transverse and parallel geometries, respectively. This procedure implies that the slowly incoming ions are evolving against a background of faster fluctuating target electrons ($V < V_{\rm the}$) providing the OCP rigid neutralizing background, thus validating the OCP assumption.

Moreover, restricting to proton projectiles impacting an electron–proton plasma [25], we immediately perceive the pertinence of the diffusion-based LIVSD as phrased by (17).

First, the proton beam can easily self diffuse amongst its target homologues, while the same mechanism experienced by target electrons allows them to drag ambipolarly the incoming proton projectiles [26].

So, the transverse electron LIVSD can be monitored either by the well-known classical diffusion $D_\perp \sim B^{-2}$ or by the Bohm-like hydrodynamic one with $D_\perp \sim B^{-1}$. In the first case, momentum conservation at the level of the electron–ion pair implies that the ions will diffuse with the same coefficient as the electrons. On the other hand, the hydro-Bohm diffusion across **B** is operated through clumps [27] with a large number of particles involved in this collective process.

Transverse $D_\perp$ and parallel $D_\parallel$ diffusion coefficients have already been discussed at length by Marchetti et al. [23] and Cohen and Suttorp [24]. Their derivation is based on the specific features of four finite-frequency and propagating hydromodes

https://doi.org/10.1017/S0022377809007934 Published online by Cambridge University Press

in a strongly magnetized OCP with the ratio of plasma to cyclotron frequencies $\omega_p/\omega_b < 1$.

First, two high-frequency modes generalize first Bernstein modes ($B = 0$) and two finite-frequency modes extend the $B = 0$ shear modes.

So, exploring first the $\omega_b \geqslant \omega_p$ domain, one can explore the parallel and B-independent diffusion [23],

$$D_{\parallel}^{(0)} = \frac{3\sqrt{\pi}V_{thi}^2}{\nu_e} \sim 0(\omega_b^0), \tag{19a}$$

yielding readily the unmagnetized ($B = 0$) LIVSD [16], where $V_{thi}^2 = k_B T/M_i$, $v_e = \omega_p \varepsilon_p \ln(1/\varepsilon_p)$ in terms of the redefined dimensionless plasma parameter $\varepsilon_p = 1/n_e\lambda_D^3$, and λ_D, the Debye length, in a beam–plasma system taken as globally neutral with $\nu_e/\omega_b \ll 1$.

At the same level of approximation, transverse diffusion reads [23]

$$D_{\perp}^{(0)} = \frac{r_L^2 \nu_e}{3\sqrt{\pi}} \sim O(\omega_b^{-2}), \tag{19b}$$

in terms of the Larmor radius $r_L = V_{thi}/\omega_b$.

With higher B values ($\omega_b \gg \omega_p$) one reaches the transverse hydro-Bohm regime featuring [23]

$$D_{\perp}^{(0)} = D_{\perp}^0 + \frac{0.5V_{thi}^2}{\omega_b}\varepsilon_p^2(\ln(1/\varepsilon_p))^{3/2}, \tag{20}$$

while parallel diffusion retains a ω_b dependence through [24]

$$D_{\parallel}^{-1} = \frac{\Gamma^{5/2}}{\omega_p a^2} \cdot \left(\frac{3}{\pi}\right)^{1/2} \cdot \left(0.5\log(1+X^2) - 0.3 + \frac{0.0235}{r^2}\right), \tag{21}$$

where $\Gamma = a^2/3\lambda_D^2$ with $a = (3/4\pi n_e)^{1/3}$, $r = \omega_p/\omega_b$, and $X = (1/\sqrt{3}\Gamma^{3/2}), \Gamma < 1$ encompassing most, if not all, situations of practical interest.

When electron diffusion is considered, V_{the} should be used in (20), and the above ambipolar process has to be implemented.

The $D_{\perp}$ and $D_{\parallel}$ expressions introduced in (17) are expected to document a strong anisotropy between transverse and parallel slowing down. However, in both cases, the B dependence is obviously increasing with B^2 (classical) or B (Bohm like). The temperature behaviour is much more intriguing, as respectively displayed in Figs. 9 and 10 for transverse and parallel LIVSD in a UCP considered for ion-beam cooling (see Fig. 6). One then witnesses a monotonic increase for transverse stopping (Fig. 9) contrasted to a monotonic decay for the parallel counterpart (Fig. 10).

As a summary, we implemented the very simple LIVSD expression (17) to the a priori very involved ion beam–arbitrarily magnetized plasma interaction. We used transverse and parallel diffusion coefficients [23,24] in suitably framed magnetized one-component plasma (OCP) with target electrons building up the corresponding neutralizing background. Thus, we reached analytic LIVSD transverse and parallel expressions advocating contrasting temperature behaviour. These quantities are of obvious significance in asserting the confinement capabilities of ultra-cold plasmas at high B values.

https://doi.org/10.1017/S0022377809007934 Published online by Cambridge University Press

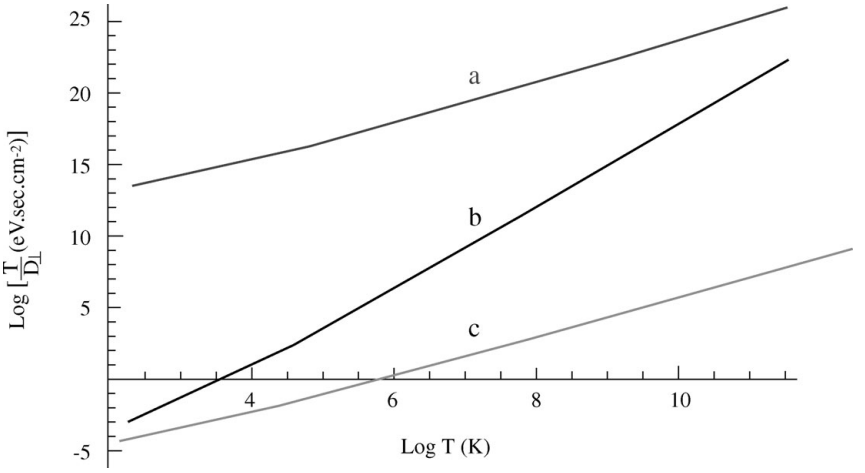

Figure 9. Proton transverse LIVSD in a cold plasma ($n = 3.5{\times}10^7$ e cm^{-3}, $10 \leqslant T$ (K) $\leqslant 10^5$, and $B = 10^4$ G) in terms of T (K). (a) Electron stopping ($D_\perp \sim B^{-2}$); (b) electron stopping ($D_\perp \sim B^{-1}$); (c) ion stopping.

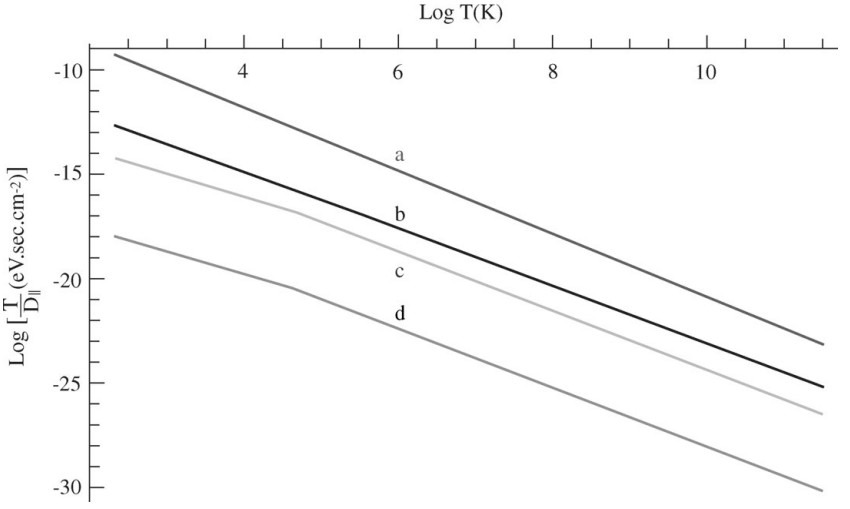

Figure 10. Proton parallel LIVSD in a cold plasma ($n = 3.5 \times 10^7$ cm^{-3} e cm^{-3}, $B = 10^4$ G), $10 \leqslant T$ (K) $\leqslant 10^5$). (a) Target ion slowing down ($B{\neq}0$); (b) target ion slowing down ($B = 0$); (c) target electron slowing down ($B{\neq}0$); (d) target electron slowing ($B = 0$). (b) and (c) stand in a log (43) ratio.

6. Conclusion and outlook

Ultra-cold plasmas (UCPs) are thus seen as offering unique opportunities for exploring the specific static and dynamic properties of strongly coupled but mostly classical electron fluids. Efficient experimental, numerical, and theoretical methodologies are presently available to converge efficiently on the completion of these goals. Interplay between laser-cooled UCPs and ion beam cooling experiments is likely to provide an interesting cross-fertilization opportunity.

https://doi.org/10.1017/S0022377809007934 Published online by Cambridge University Press

Numerical MD and Monte Carlo simulations exhibit possible reticulated Rydberg electron and ion phases, distinct from crystalline OCP, which could be explored in the laboratory.

An expanding classical electron fluid could be specifically diagnosed through low velocity ion stopping.

UCPs can be easily magnetized. This affords a unique opportunity for probing ion stopping in the rather extreme location of the target space parameters, with the electron cyclotron radius much smaller than the corresponding Debye length. Then, one expects the OCP hydromodes to play a dominant role (Sec. 5). Other topics not explored here include the recombination–ionization mechanisms under a strong imposed magnetic field.

Acknowledgement

Part of this work has been supported by the Euratom–CEA contract no. 3599.001.

References

[1] Vitrant, G., Raimond, J. M., Gross, M. and Haroche, S. 1982 Rydberg to plasma evolution in a dense gas of very excited atoms. *J. Phys.* B **15**, L49–55.

[2] Killian, T. C., Kulin, S., Bergeson, S. D., Orozec, L. A. and Rolston, S. L. 1999 Creation of an ultracold neutral plasma. *Phys. Rev. Lett.* **83**, 4776–4779.

[3] Kulin, S., Killian, T. C., Bergeson, S. D. and Rolston, S. L. 2000 Plasma oscillations and expansion of an ultracold plasma. *Phys. Rev. Lett.* **85**, 318–321.

[4] Killian, T. C., Lin, M., Kulin, S., Bergeson, S. D. and Rolston, S. L. 2001 Formation of Rydberg atoms in an expanding ultracold neutral plasma. *Phys. Rev. Lett.* **86**, 3759–3762.

[5] Robinson, M. P., Laburthe Tolra, N., Noel, M. W., Gallagher, T. F. and Pillet, P. 2000 Spontaneous evolution of Rydberg atoms into an ultracold plasma. *Phys. Rev. Lett.* **85**, 4466–4469.

[6] Killian, T. C., Ashoka, V. S., Gupta, P., Caha, S., Nagel, S. B., Simien, C. E., Kulin, S., Rolston, S. L. and Bergeson, S. D. 2003 Ultracold neutral plasmas:Recent experiments and new prospects. *J. Phys.* A **36**, 6077–6085.

[7] Keller, M. L., Anderson, L. W. and Lin Chun, C. 2000 Electron-impact ionization crose-section measurements out of the 5 2P excited state of Rubidium. *Phys. Rev. Lett.* **85**, 3353–3356.

[8] Li, W., Tanner, P. J. and Gallagher, T. F. 2005 Dipole-dipole excitation and ionization in an ultracold gas of Rydberg atoms. *Phys. Rev. Lett.* **94**, 173001.

[9] Comparat, D., Vogt, T., Nahzam, N., Mudrich, M. and Pillet, P. 2005 Star cluster dynamics in a laboratory: Electrons in an ultracold plasma. *Mon. Not. R. Astron. Soc.* **361**, 1227–1242.

[10] Gouedard, C. and Deutsch, C. 1978 Dense electron-gas response at any degeneracy. *J. Math. Phys.* **19**, 32–40.

[11] Zwicknagel, G. 1994 Energie Verlust Schwerer Ionen in Stark Gekoppelten Plasmen.Ph.D thesis. Theoretische Physik II, University of Erlangen.

[12] Deutsch, C. 1977 Nodal expansion in a real matter plasma. *Phys. Lett.* A **30**, 317–319. Deutsch, C., Furutani, Y. and Gombert, M. M. 1981 Nodal expansions for strongly coupled classical plasmas. *Phys. Rep.* **69**, 86–193.

[13] Stringfellow, G. S., DeWitt, H. E. and Slattery, W. L. 1990 Equation of state for the one-component-plasma derived from precise Monte-Carlo simulations. *Phys. Rev.* A **41**, 1105–1111.

[14] Bonitz, M., Zelener, B., Zelener, B. V., Manykin, E. A. N., Filinov, V. S. and Fortov, V. E. 2004 Thermodynamics and correlation functions of an ultracold nonideal Rydberg plasma. *JETP* **98**, 719–727.

https://doi.org/10.1017/S0022377809007934 Published online by Cambridge University Press

[15] Shumway, J. and Ceperley, D. M. 2000 Path integral Monte-Carlo simulations for fermion systems: Pairing in the electron-hole plasma. *J. Phys. IV Fr.* **10**, 3–16.

[16] Zwicknagel, G., Toepffer, C. and Reinhard, P. G. 1999 Stopping of heavy ions in plasmas at strong coupling. *Phys. Rep.* **309**, 117–208; Erratum 1999 *Phys. Rep.* **314**, 671.

[17] Zwicknagel, G. 2001 Nonlinear energy loss of heavy ions in plasma. *Nucl. Instrum. Methods* B **197**, 22–38.

[18] Robichaux, F. and Hanson, J. D. 2002 Simulation of the expansion of an ultracold plasma. *Phys. Rev. Lett.* **88**, 055002.

[19] Bret, A. and Deutsch, C. 1993 Dielectric response function and stopping power of a two-dimansional electron-gas. *Phys. Rev.* E **48**, 2994–3002.

[20] Nersisyan, H. B., Toepffer, C. and Zwicknagel, G. 2007 *Interaction Between Charged Particles in a Magnetic Field*. Springer-Verlag, Berlin-Heidelberg.

[21] Dufty, J. M. and Berkovsky, M. 1995 Electronic stopping of ions in the low velocity limit. *Nucl. Instrum. Methods Phys. Res.* B **96**, 626–632.

[22] A fundamental restriction on the relations (17) arises a priori from the strong inequality $M_{\mathrm{p}}/m \gg 1$ between ion projectile and electron masses. However, Dufty and Berkovsky [21] demonstrated how it can be considerably relaxed.

[23] Marchetti, M. C., Kikpatrick, T. R. and Dorfman, J. R. 1987 Hydrodynamic theory of electron transport in a strong magnetic field. *J. Statist. Phys.* **46**, 679–708; Erratum 1987 *J. Stat. Phys.* **49**, 871–872.

Marchetti, M. C., Kikpatrick, T. R. and Dorfman, J. R. 1984 Anomalous diffusion of charged particles in a strong magnetic field. *Phys. Rev.* **A29**, 2960–2962.

[24] Cohen, J. S. and Suttorp, L. G. 1984 The effect of dynamical screening on self-diffusion in a dense magnetized plasma. *Physica* **126A**, 308–327.

[25] The extension to a more general ion beam–plasma system requires us to replace the OCP by a binary ionic mixture (BIM) modelization.

[26] Goldston, R. J. and Rutherford, P. H. 1995 *Introduction to Plasma Physics*. Institute of Physics, Philadelphia, p. 318.

[27] Montgomery, D., Liu, C. S. and Vahala, G. 1972 Three-dimensional plasma diffusion in a very strong magnetic field. *Phys. Fluids* **15**, 815–819.

https://doi.org/10.1017/S0022377809007934 Published online by Cambridge University Press